# Supporting Information for Quantifying the Internal and External Drivers of Southeast Asian Rainfall Extremes on Decadal Timescales

Shawn Wang [1,2], Caroline C. Ummenhofer[2], Sujata A. Murty[3], Hung T.T. Nguyen[4], Brendan M. Buckley[4]

[1]MIT-WHOI Joint Program in Oceanography, Cambridge, MA, USA

[2]Woods Hole Oceanographic Institution, Woods Hole, MA, USA

[3]University at Albany, State University of New York, Albany, NY, USA

[4]Lamont-Doherty Earth Observatory, Columbia University, Palisades, NY, USA

## Contents of this file

1. Table S1 to S2
2. Figures S1 to S9

Corresponding author: S. Wang, Woods Hole Oceanographic Institution, Woods Hole, MA (syiwang@mit.edu)

**Table S1.** Pearson correlation coefficient between bandpass (10-50 years) filtered climate indices in CESM-LME (13 all-forcing ensemble members). Climate indices are constructed from annual SST values using regions described in section 2.1.

| | IPO | ENSO | IOD |
|---|---|---|---|
| IPO | 1 | 0.94 | 0.64 |
| ENSO | 0.94 | 1 | 0.55 |
| IOD | 0.61 | 0.55 | 1 |

**Table S2.** Slope values from partial regression (added variable) analysis between decadal-filtered IPO, IOD, and MSEA rainfall without any binning into quantiles. Slopes are computed for dry anomalies (drought) and wet anomalies (pluvial) separately. In addition to computing them for the all-forcing LME (AF), we compute partial regression for the LME with the ensemble mean removed, similar to Section 5 analysis. ** denotes slope values significant at the 5% using phase-scrambling Monte-Carlo simulations.

| | Drought (AF) | Pluvial (AF) | Drought (IC) | Pluvial (IC) |
|---|---|---|---|---|
| IPO | -37** | -31** | -31** | -28** |
| IOD | 2 | -11 | -7 | -12** |

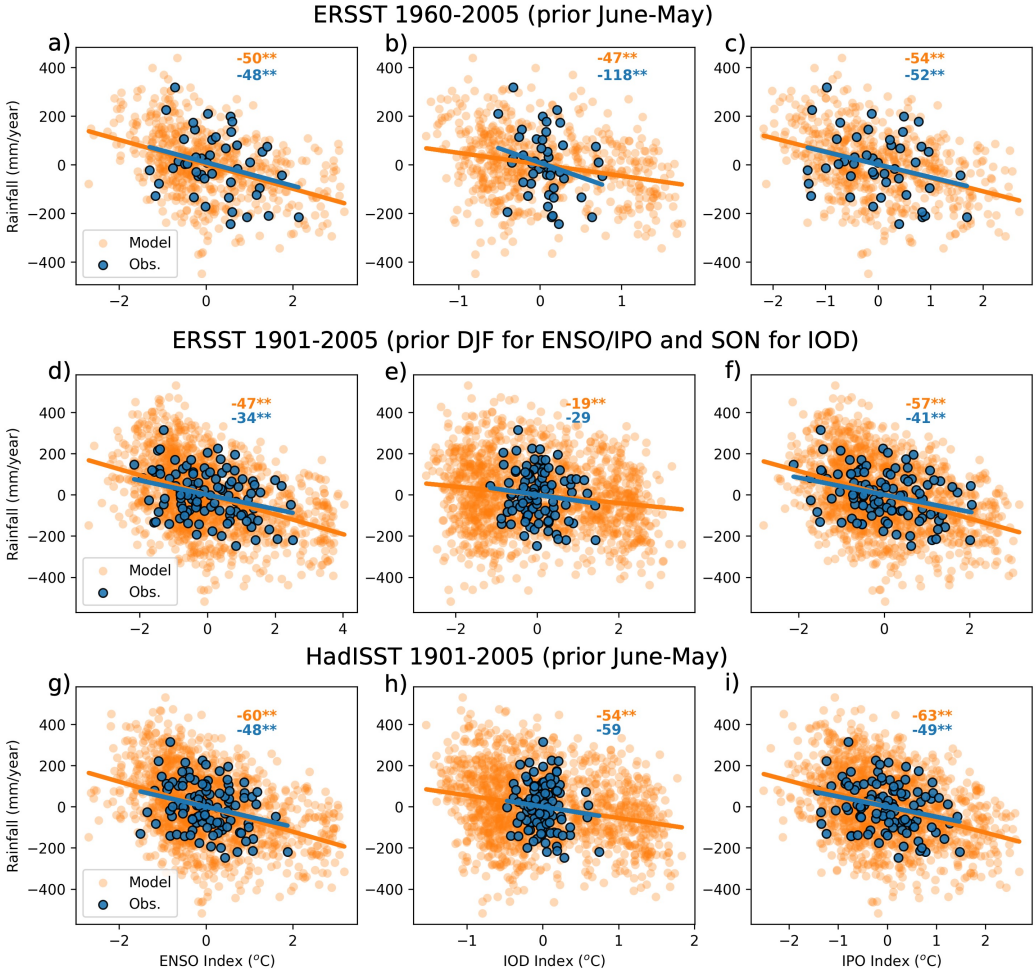


**Figure S1.** The relationship between ENSO **(a,d,g)**, IOD **(b,e,h)**, and IPO **(c,f,i)** and MSEA rainfall are shown for observations (blue) and model (orange) for individual years (scatterpoints) and linear regression (line) with regression slope shown (numbers) for various time-intervals and observational datasets. Scatterplots are shown using ERSST and averaging over the preceding hydrological year (prior June-May) for the climate mode anomalies over the 1960-2005 period in the top row **(a,b,c)**. Scatterplots are shown using ERSST and averaging over the prior December-February (DJF) for ENSO/IPO and September-November (SON) for IOD over the 1901-2005 period in the middle row **(d,e,f)**. Scatterplots are shown using HadISST and averaging over the preceding hydrological year (prior June-May) for the climate mode anomalies over the 1901-2005 period in the bottom row **(g,h,i)**. ** denotes significant at the 5% from phase scrambling. Data from all 13 CESM all-forcing ensemble members are utilized here

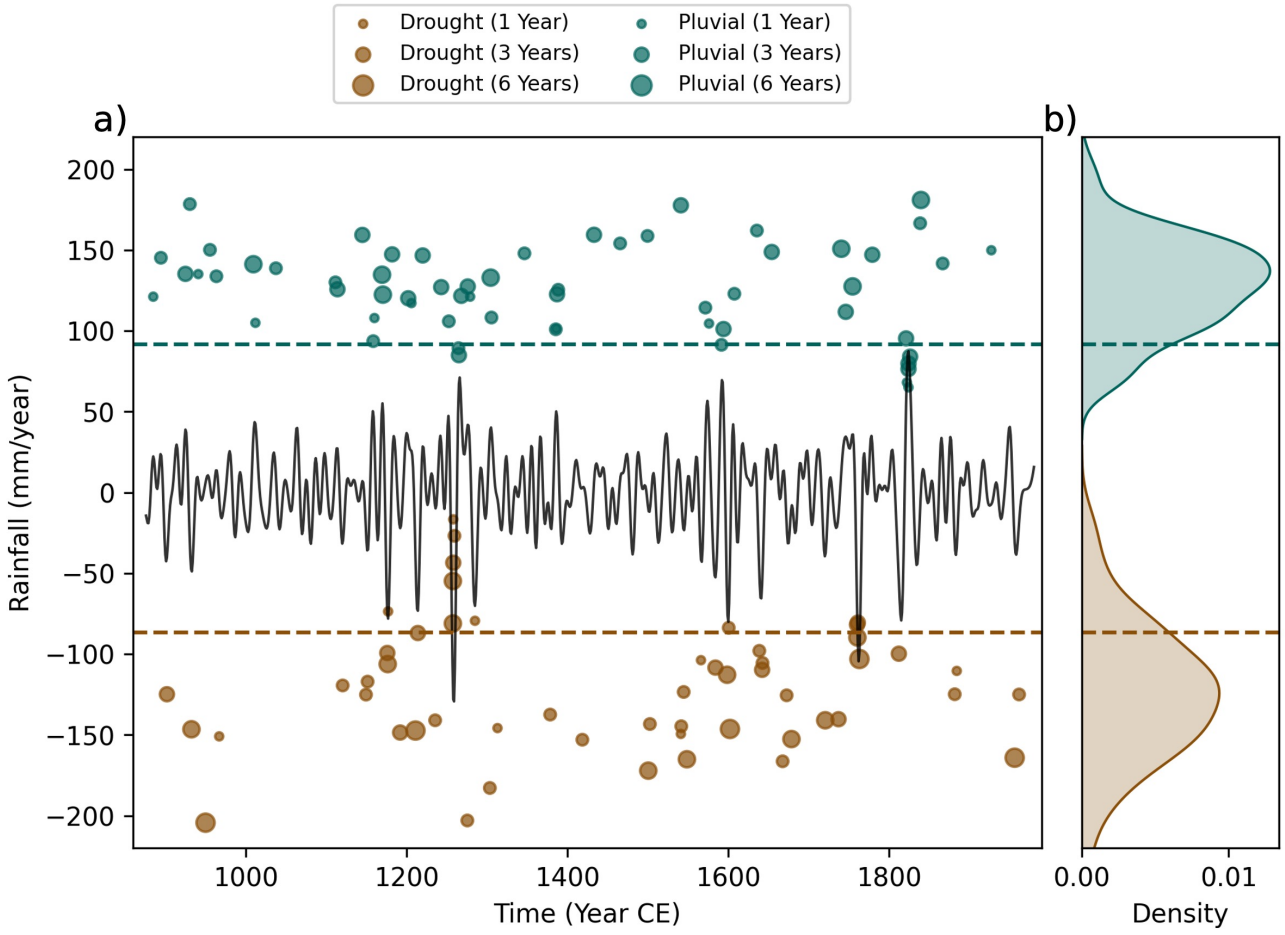


**Figure S2.** Drought (brown circles) and pluvial (green circles) extremes magnitude, determined using a 2% threshold, associated with internal variability ($R_{IC}$) along with the ensemble mean rainfall anomaly (black line) over the last millennium **(a)**. The size of the circles scales with the length of the rainfall extreme, ranging from 1-6 years. The PDF distribution of $R_{IC}$ values for all drought and pluvial extremes **(b)**. Brown (green) dashed lines correspond to the 5% significance threshold of $R_{IC}$ for drought (pluvial) extremes determined from phase scrambling.

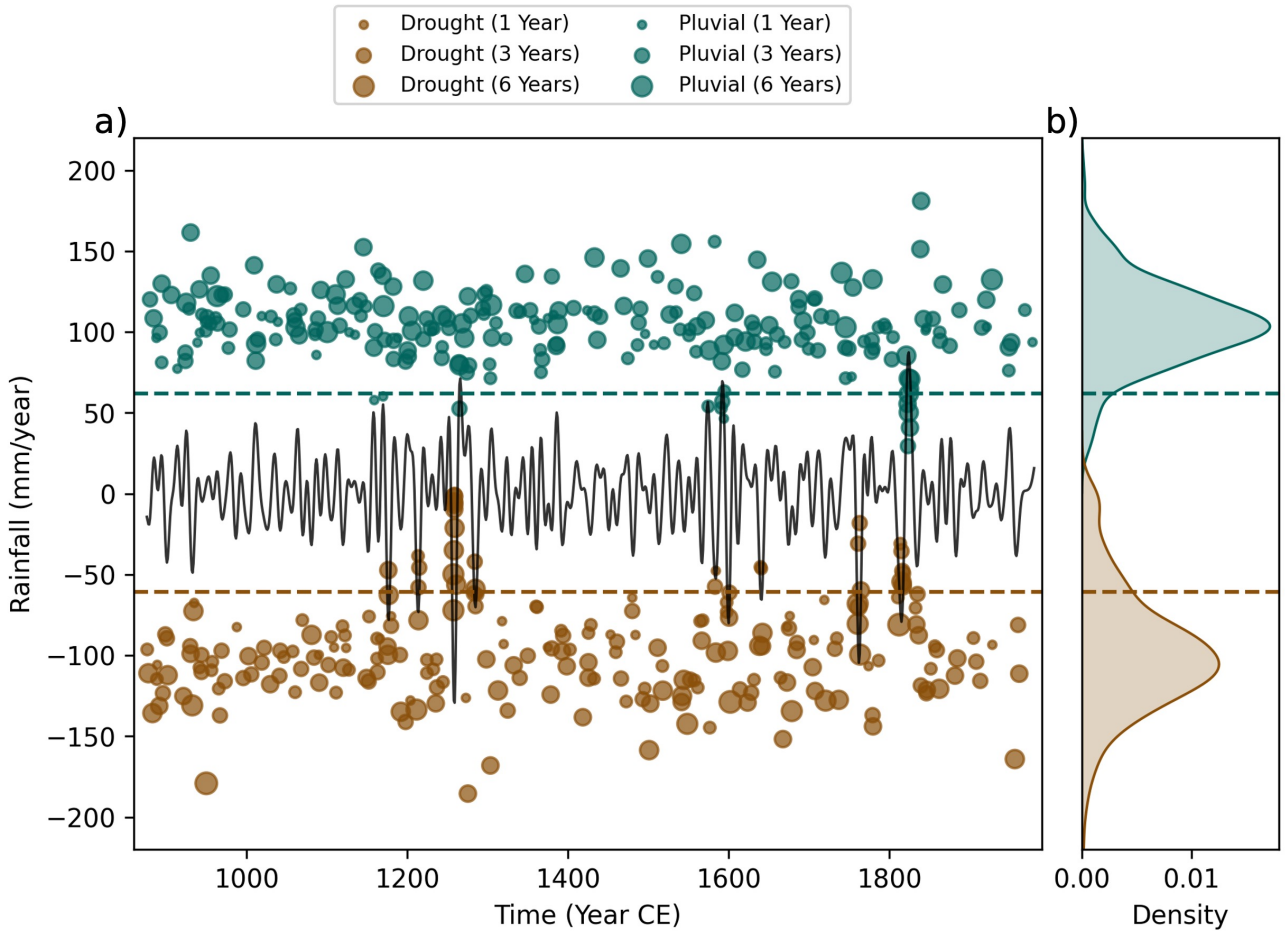


**Figure S3.** Drought (brown circles) and pluvial (green circles) extremes magnitude, determined using a 10% threshold, associated with internal variability ($R_{IC}$) along with the ensemble mean rainfall anomaly (black line) over the last millennium **(a)**. The size of the circles scales with the length of the rainfall extreme, ranging from 1-6 years. The PDF distribution of $R_{IC}$ values for all drought and pluvial extremes **(b)**. Brown (green) dashed lines correspond to the 5% significance threshold of $R_{IC}$ for drought (pluvial) extremes determined from phase scrambling.

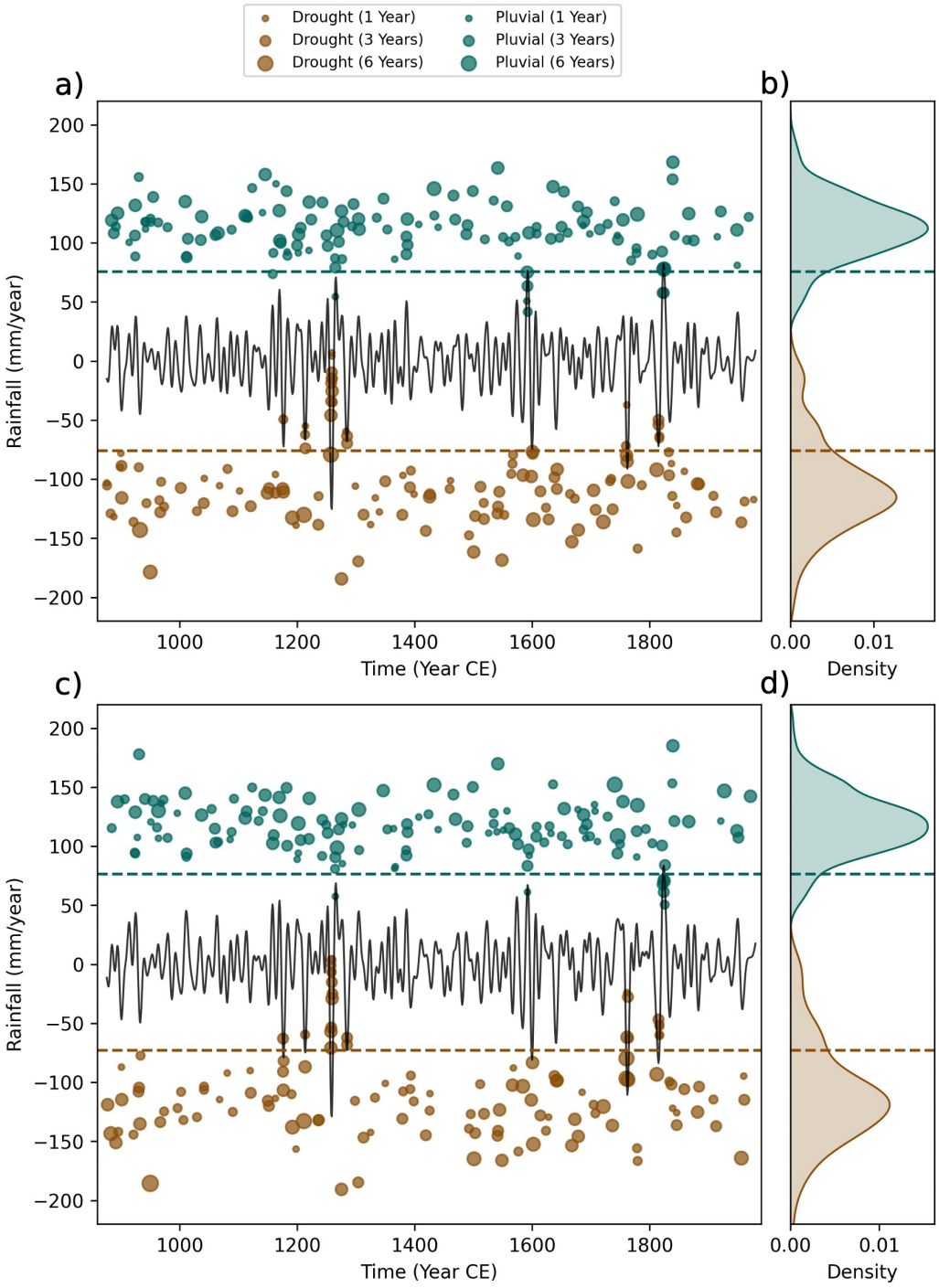


**Figure S4.** Identical to Figure 3 analysis except using a 10-40 year bandpass filter window **(a,b)** and a 10-60 year bandpass filter window **(c,d)** for all LME data

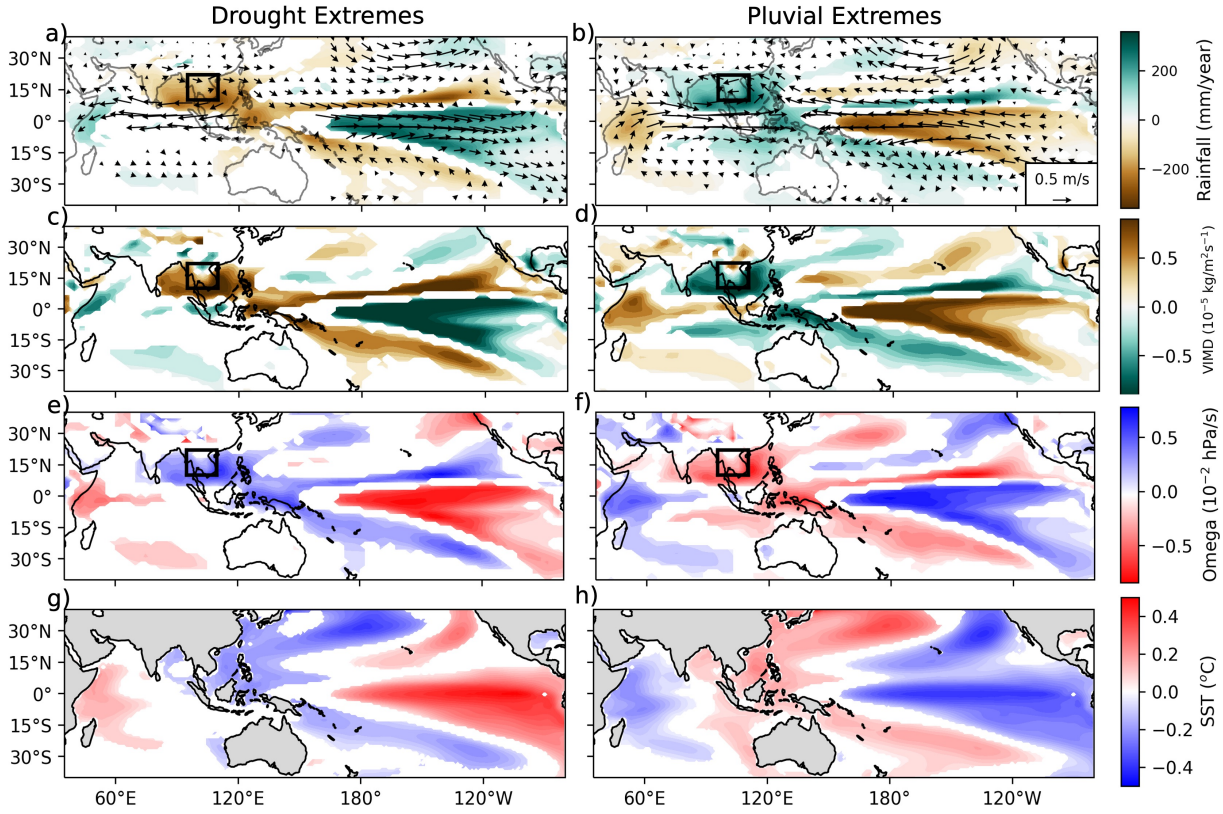


**Figure S5.** Composite rainfall (colors) and 850 hPa wind anomalies (vectors) during MSEA drought **(a)** and pluvial **(b)** extremes using a 2% threshold. Vertically integrated moisture divergence (VIMD) in the lower troposphere (1000-700 hPa) anomalies during drought **(c)** and pluvial **(d)** extremes. Vertical velocity anomalies at 700 hPa during drought **(e)** and pluvial **(f)** intervals. SST anomalies during drought **(g)** and pluvial **(h)** extremes. SST anomalies are shown for the hydrological year leading up to rainfall extremes (prior June-May) while all other variables are derived for the calendar year of rainfall extremes. All results are shown for the 13 all-forcing LME ensemble members. Black box in **(a-f)** corresponds to MSEA region used to define extremes. Only anomalies significant at the 5% are shown using phase-scrambling Monte-Carlo simulations.

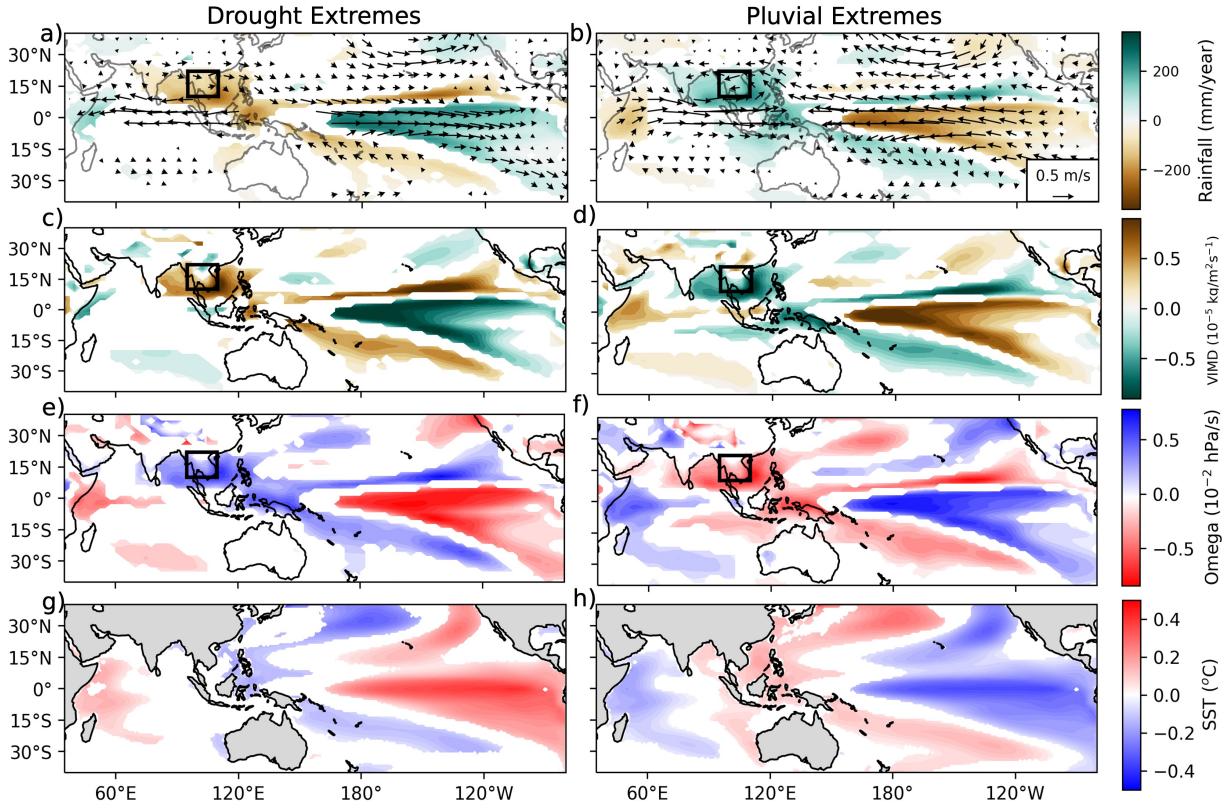


**Figure S6.** Composite rainfall (colors) and 850 hPa wind anomalies (vectors) during MSEA drought **(a)** and pluvial **(b)** extremes using a 10% threshold. Vertically integrated moisture divergence (VIMD) in the lower troposphere (1000-700 hPa) anomalies during drought **(c)** and pluvial **(d)** extremes. Vertical velocity anomalies at 700 hPa during drought **(e)** and pluvial **(f)** intervals. SST anomalies during drought **(g)** and pluvial **(h)** extremes. SST anomalies are shown for the hydrological year leading up to rainfall extremes (prior June-May) while all other variables are derived for the calendar year of rainfall extremes. All results are shown for the 13 all-forcing LME ensemble members. Black box in **(a-f)** corresponds to MSEA region used to define extremes. Only anomalies significant at the 5% are shown using phase-scrambling Monte-Carlo simulations.

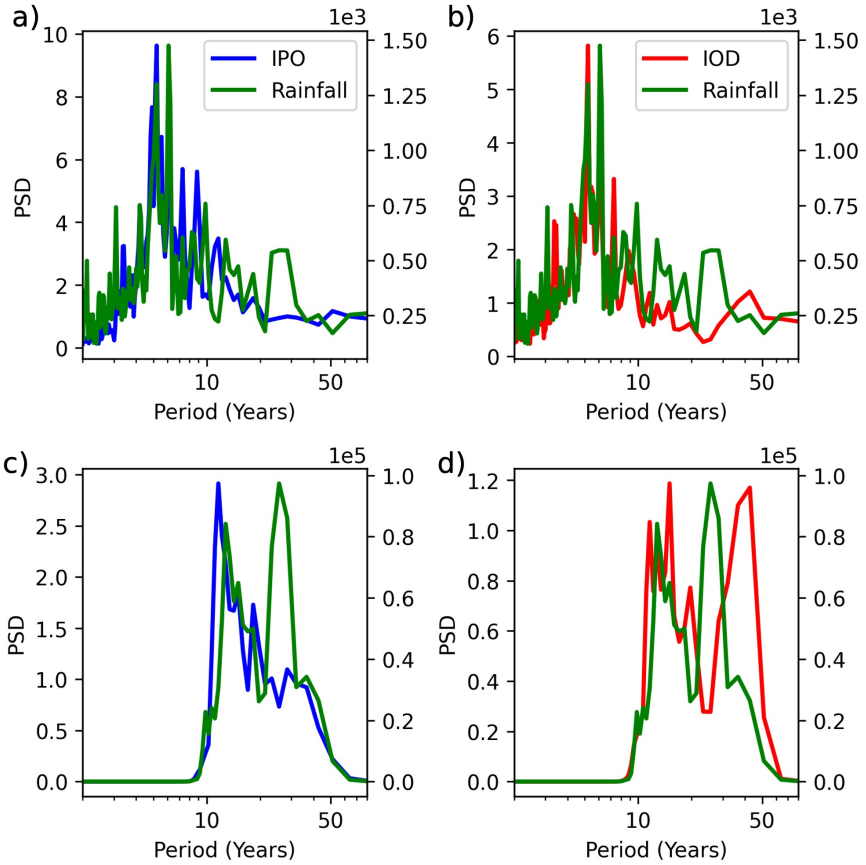


**Figure S7.** Power spectral density (PSD) of timeseries of MSEA rainfall (green) compared to timeseries of IPO **(a,c)** and IOD **(b,d)** both without bandpass filter (top row) and with the decadal bandpass filter (bottom row). Results are shown for 850-2005 CE for ensemble member 1 of the LME. Similar results are found for other ensemble members of the LME (not shown)

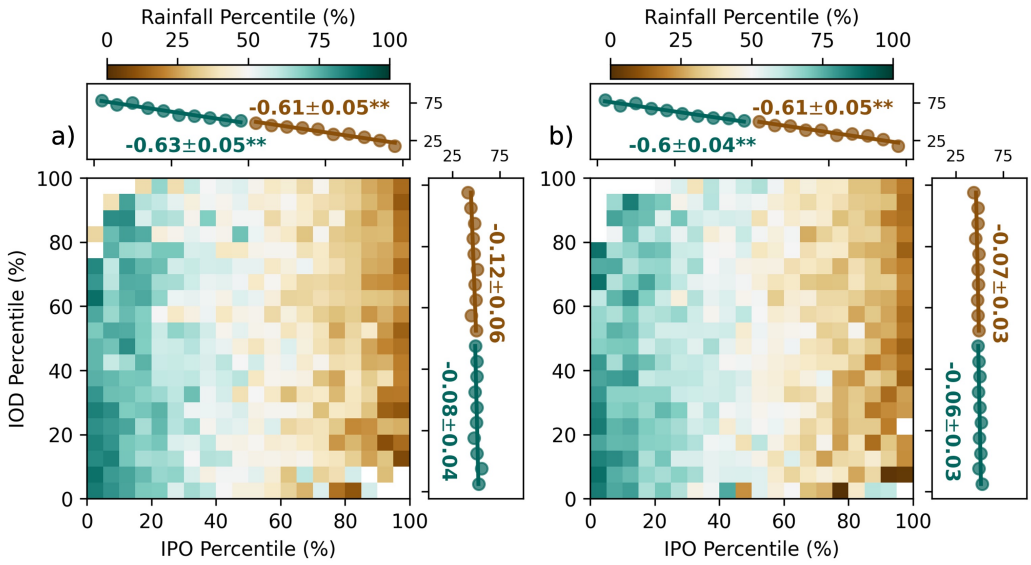


**Figure S8.** Identical to Figure 7 analysis except using a 10-40 year bandpass filter window **(a)** and a 10-60 year bandpass filter window **(b)** for all LME data.

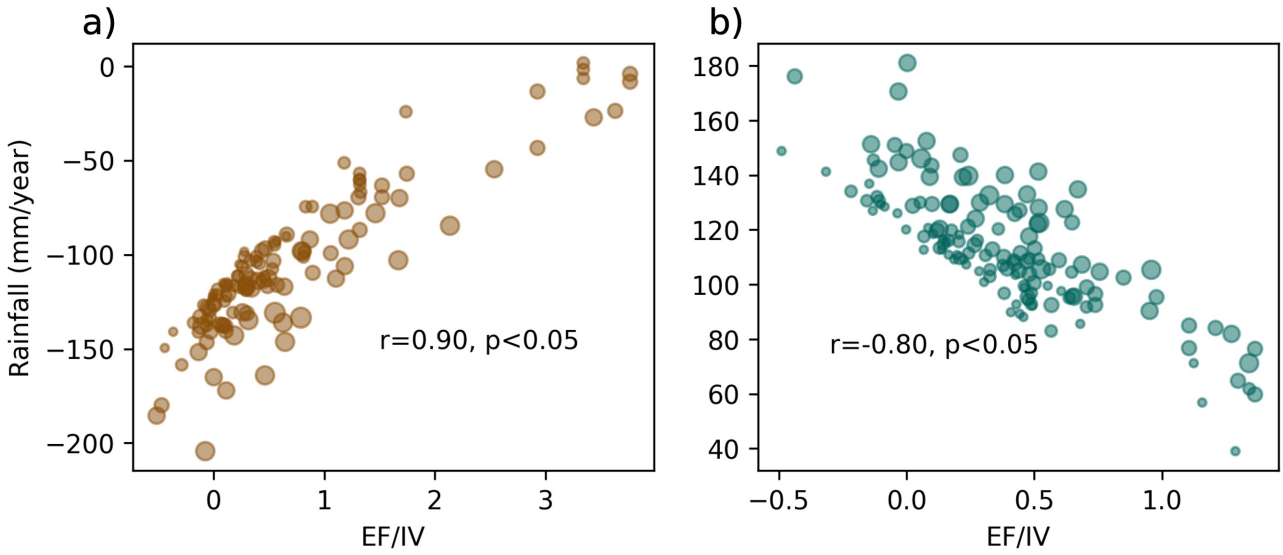


**Figure S9.** The relationship between the EF/IV and $R_{IC}$ (internal contribution to rainfall) for MSEA droughts **(a)** and pluvials **(b)** identified using the 5% threshold for rainfall extremes. The Pearson correlations and their significance (r and p values) between EF/IV and $R_{IC}$ are also shown.